Geophys. J. Int. (2008)

An efficient method to compute the dynamic response of a fluid-filled crack

Mare Yamamoto* and Hitoshi Kawakatsu
Earthquake Research Institute, University of Tokyo, Tokyo 113-0032, Japan. E-mail: mare@zisin.geophys.tohoku.ac.jp

Received 2008 March 23; in original form 2007 October 12

SUMMARY

The vibration of a fluid-filled crack is considered to be one of the most plausible source mechanisms for the long-period events and volcanic tremors occurring around volcanoes. As a tool for the quantitative interpretation of source process of such volcanic seismic signals, we propose a method to numerically simulate the dynamic response of a fluid-filled crack. In this method, we formulate the motions of the fluid inside and the elastic solid outside of the crack using boundary integrals in the frequency domain, and solve the dynamic interactions between the fluid and the elastic solid using the point collocation method. The present method is more efficient compared to the time-domain finite difference method which has been used in simulations of a fluid-filled crack, and enables us to study the dynamics of a fluid-filled crack over a wide range of physical parameters. The method also allows us direct calculation of the attenuation quality factor of the crack resonance which is an indispensable parameter for estimating the properties of the fluid inside the crack. The method is also designed to be flexible to many applications which may be encountered in volcano seismology, and thus extensions of the method to more complicated problems are promising.

Key words: volcanic earthquakes; crack model; fluid composition; crack wave

1 INTRODUCTION

Spectra of volcanic earthquakes and tremors often show a series of narrow peaks which are sometimes regularly spaced. Such spectra naturally invoke an idea of oscillations of some resonant system, and from this point of view, most of the current models and theories consider these volcanic signals are generated by the acoustic resonances of bodies and/or networks of volcanic fluids (e.g., Kawakatsu & Yamamoto, 2007). These models include resonances of fluid inclusions that having spherical (e.g., Fujita et al., 1995; Sakuraba et al., 2002), cylindrical/pipe-like (e.g., Ferrick et al., 1982; Chouet, 1985), and crack-like (e.g., Aki et al., 1977; Chouet, 1986, 1988) shapes.

Among the family of resonance models of fluid inclusions, the fluid-filled crack model is widely accepted as a source model for shallow volcanic seismic signals. The dynamics of a fluid-filled crack has been extensively studied by many researchers after the pioneering work by Aki et al. (1977), and it has been revealed that observed spectral and oscillatory characteristics are quantitatively well explained by the model. Chouet (1986) numerically studied the dynamics of a fluid-filled crack by solving the equations of motion of the fluid inside the crack and the surrounding elastic solid simultaneously using three-dimensional (3-D) time-domain finite-difference method (hereafter FDTD), and found the existence of a wave named 'crack wave' which propagates with a slower velocity compared to the acoustic velocity of the fluid. As analytically demonstrated by Krauklis (1962) and Ferrazzini & Aki (1987) for the case of an infinite fluid layer between two elastic half-spaces, the crack wave is generated by the interference of two Stoneley modes propagating in the fluid and elastic solid, and the essential nature of the crack wave is same as those of the tube wave in a cylindrical bore (e.g., Biot, 1952) and the slow wave in periodically stratified solid and fluid layers (e.g., Schoenberg & Sen, 1983).

The slow propagation nature of the crack wave provides a natural explanation for the low-frequency characteristics of observed volcanic seismic signals, and the model has been applied to interpret these signals at many volcanoes around the world (c.f., Chouet, 2003). For example, the long-period tremor observed at Aso volcano, Japan, which has a fundamental period of 15 sec (e.g., Kawakatsu et al., 2000) could be explained by the oscillation of a crack-like conduit having a dimension of about 1 km; such conduit was detected by a dense broadband seismic network (Yamamoto et al., 1999). Kumagai & Chouet (2000) further studied the response of a fluid-filled crack with

*Now at Department of Geophysics, Tohoku University, Sendai, Japan

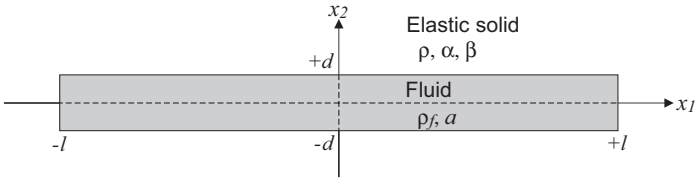

Figure 1. Configuration of the problem. A thin crack whose length and thickness are $2l$ and $2d$ is embedded in an infinite elastic medium. The thickness of the crack is assumed to be much smaller than the seismic wavelength of interest. ρ and ρ_f are densities of the elastic solid and fluid, and α, β, a represent the compressional and shear velocities of the solid and acoustic velocity of the fluid, respectively.

various physical properties in a systematic manner using 3-D FDTD developed by Chouet (1986), and demonstrated a way to quantitatively infer the fluid properties from observed complex frequencies. Their method has been successfully applied to studies of volcanic signals observed at Kusatsu-Shirane volcano (Kumagai et al., 2002), Hachijo Island (Kumagai et al., 2003) in Japan, Tungurahua volcano in Ecuador (Molina et al., 2004), and Mt. Spurr in Alaska (De Angelis & McNutt, 2005).

As applications of the model become more sophisticated, however, some issues inherent to the numerical method arise. One is the difficulty in quantitatively estimating an attenuation quality factor of the oscillation in the time-domain calculation; another is the efficiency and stability of the computations, that is FDTD requires calculation over whole computational region at each time step, and also requires discretization both in space and time depending on the material properties to meet the stability condition. In addition to these, it is rather difficult to extend the FDTD to problems that include the frequency-dependent properties of materials as often appear in volcanic processes such as the dynamics of fluids containing gas bubbles. Of course, there are several methods for overcoming these limitations such as the use of the variable grid and the memory variables (e.g., Carcione et al., 2002). Nevertheless, such procedures generally contain some physical assumptions inherent to their numerical approach, and it may not be suitable to use them in a systematic study of the dynamics of a fluid-filled crack over a wide range of parameters.

To overcome the above-mentioned limitations of FDTD, we introduce in this paper a simple alternative method to simulate the dynamics of a fluid-filled crack using the frequency-domain boundary integral method. The boundary integral method is based on the formulation of governing equations in terms of integral equations on boundaries, and the method has been widely used in seismology and geophysics. Applications include modeling of wave scattering by cracks and heterogeneous structures (e.g., Benites et al., 1992) and modeling of borehole modes in a borehole with arbitrary cross sections (e.g., Randall, 1991). Various kinds of approaches have also been proposed to solve a set of integral equations.

In this paper, for simplicity, we describe only the infinite 2-D steady-state problem, although the extensions of the present method to the semi-infinite 2-D problem and/or 3-D problem are straightforward, and we already confirmed the applicability of the procedure to the 3-D problem,

2 FORMULATION OF THE PROBLEM

We consider a rectangular fluid-filled crack with a length of $2l$ and a thickness of $2d$ embedded in an infinite homogeneous isotropic elastic medium (Fig. 1). The crack is filled with an inviscid fluid whose density and acoustic velocity are ρ_f and a, and is surrounded by an elastic solid medium whose density, compressional and shear velocities are ρ, α, and β, respectively. The thickness of the crack is assumed to be much smaller than the seismic wavelength of interest.

Our goal in the present study is to develop an efficient and stable method for simulating the dynamic response of a fluid-filled crack over a wide range of material properties. In this method, the elastic interaction between the fluid and surrounding elastic solid is thus simulated in the frequency domain. Our procedure consists of two steps: First, for each media inside and outside of the crack, we derive expressions of the motion as integrals of the displacement on the crack surface. Second, we determine the distribution of the crack surface displacement so that the continuity of stresses across the fluid-solid interfaces are satisfied.

In the following sections, as an example of the formulation of a fluid-filled crack, the symmetric motion of a fluid-filled crack about the crack plane is considered.

2.1 System of equations

Boundary integral representation of the motion in the elastic solid region

From the representation theorem of the elastodynamics (e.g., Aki & Richards, 2002), in the frequency domain, we can write the displacement $\boldsymbol{u}$ at any point $\boldsymbol{x}$ in the surrounding elastic solid due to the displacement $\boldsymbol{w}$ on the crack surface as

$$u_i(\boldsymbol{x}) = \int_{-l}^{+l} \Delta w_j(\boldsymbol{\xi}) n_k c_{jklm} G_{il,m}(\boldsymbol{x}, \boldsymbol{\xi})\, d\xi, \tag{1}$$

where u_i is the displacement in x_i-th direction and $\Delta w_j(\boldsymbol{\xi})$ is the x_j-th component of the displacement discontinuity across the crack plane at a point $\boldsymbol{\xi}$ along the crack surface ($\Delta w_j = w_j^+ - w_j^-$ where ${w_j}^{\pm}$ represents the displacement on the two facing surfaces of the rectangular crack). n_k is the k-th component of the normal vector $\boldsymbol{n}$ of the crack surface, c_{jklm} is the elastic constant tensor, and G_{il} is the Green's tensor of the elastic solid, respectively, and $G_{il,m}$ represents the partial derivative of G_{il} with respect to ξ_m. For the 2-D infinite isotropic problem, the Green's function is given by

$$G_{il}(\boldsymbol{x},\boldsymbol{\xi}) = \frac{i}{4\pi\rho\omega^2}\left[k_\beta^2 H_0^{(1)}(k_\beta r)\delta_{ij} + \left\{H_0^{(1)}(k_\beta r) - H_0^{(1)}(k_\alpha r)\right\}_{,il}\right], \quad r = |\boldsymbol{x}-\boldsymbol{\xi}|, \tag{2}$$

where $\omega, k_\alpha, k_\beta$ are the angular frequency and wave numbers of the compressional and shear waves, respectively, and $H_0^{(1)}$ is the zeroth order Hankel function of the first kind (e.g., Banerjee & Butterfield, 1979).

Assuming that the tangential displacement of the crack surface is small, we may rewrite Eq. (1) using the displacement discontinuity Δw_2 normal to the crack plane as

$$u_i(\boldsymbol{x}) = \int_{-l}^{+l} \Delta w_2(\boldsymbol{\xi}) T_{i2}^{(2)}(\boldsymbol{x},\boldsymbol{\xi})\, d\xi, \tag{3}$$

using the traction Green's function defined by $T_{ij} \equiv n_k c_{jklm} G_{il,m}(\boldsymbol{x},\boldsymbol{\xi})$. In Eq. (3), $T_{ij}^{(k)}$ represents $T_{ij}^{(k)} = n_k c_{jklm} G_{il,m}(\boldsymbol{x},\boldsymbol{\xi})$ without the summation rule with respect to k. Similarly, the spatial derivatives of displacement can be written as

$$\begin{aligned} u_{i,1}(\boldsymbol{x}) &= \int_{-l}^{+l} \Delta w_{2,1}(\boldsymbol{\xi}) T_{i2}^{(2)}(\boldsymbol{x},\boldsymbol{\xi})\, d\xi, \\ u_{i,2}(\boldsymbol{x}) &= -\int_{-l}^{+l} \Delta w_{2,1}(\boldsymbol{\xi}) T_{i2}^{(1)}(\boldsymbol{x},\boldsymbol{\xi})\, d\xi + \rho\omega^2 \int_{-l}^{+l} \Delta w_2(\boldsymbol{\xi}) G_{ij}(\boldsymbol{x},\boldsymbol{\xi})\, d\xi, \end{aligned} \tag{4}$$

and the corresponding stresses in the elastic solid become

$$\begin{aligned} \tau_{12}(\boldsymbol{x}) =& \mu\Big[\int_{-l}^{+l} \Delta w_{2,1}(\boldsymbol{\xi}) \left\{T_{22}^{(2)}(\boldsymbol{x},\boldsymbol{\xi}) - T_{12}^{(1)}(\boldsymbol{x},\boldsymbol{\xi})\right\} d\xi + \rho\omega^2 \int_{-l}^{+l} \Delta w_2(\boldsymbol{\xi}) G_{12}(\boldsymbol{x},\boldsymbol{\xi}) d\xi\Big], \\ \tau_{22}(\boldsymbol{x}) =& \lambda \int_{-l}^{+l} \Delta w_{2,1}(\boldsymbol{\xi}) T_{12}^{(2)}(\boldsymbol{x},\boldsymbol{\xi}) d\xi + (\lambda+2\mu)\left\{-\int_{-l}^{+l} \Delta w_{2,1}(\boldsymbol{\xi}) T_{22}^{(1)}(\boldsymbol{x},\boldsymbol{\xi}) d\xi + \rho\omega^2 \int_{-l}^{+l} \Delta w_2(\boldsymbol{\xi}) G_{22}(\boldsymbol{x},\boldsymbol{\xi}) d\xi\right\}, \end{aligned} \tag{5}$$

where λ, μ are the Lame's constants corresponding to the elastic constant c_{jklm} of the homogeneous isotropic medium. Since Eqs. (3) and (5) are general expressions for the displacements and stresses at any point within the elastic solid, we can obtain stresses on the crack surface by taking the limit of $x_2 \to 0$.

Here, it should be noticed that, by taking the limit, Eq. (5) becomes singular since $H_0^{(1)}(kr)$ diverges in the limit of $r = |\boldsymbol{x}-\boldsymbol{\xi}| \to 0$. However, considering that the displacement and traction Green's functions (G and T) contain only terms in the form of $H_0^{(1)}(kr)$ as shown in Eq. (2), the asymptotic behavior of G and T in the limit of $r \to 0$ are the same as those of $kr \to 0$. This means that the static Green's functions can be used to calculate the limit of $r \to 0$ rather than the elastodynamic Green's functions. The static Green's functions in 2-D are given by (e.g., Banerjee & Butterfield, 1979)

$$\begin{aligned} G_{ij}(\boldsymbol{x},\boldsymbol{\xi}) &= \frac{1}{8\pi\mu(1-\nu)}\left\{-(3-4\nu)\delta_{ij}\log r - \hat{r}_i\hat{r}_j\right\}, \\ T_{ij}(\boldsymbol{x},\boldsymbol{\xi}) &= \frac{1}{4\pi(1-\nu)}\,\frac{1}{r}\left[(1-2\nu)(n_j\hat{r}_i - n_i\hat{r}_j) + \left((1-2\nu)\delta_{ij} + 2\hat{r}_i\hat{r}_j\right) n_k\hat{r}_k\right], \\ \hat{r}_i &= \frac{(x_i-\xi_i)}{r}, \end{aligned} \tag{6}$$

where ν is the Poisson's ratio of the elastic solid. From these equations, it is clearly seen that the singularities involved in the Green's functions are of the order of $\log r$ and $1/r$. The former singularity is weak and can be computed by numerical means, and the latter one can be evaluated as the Cauchy principal value.

Boundary integral representation of the motion in the fluid region

The equation of momentum and the equation of continuity for the inviscid fluid inside the crack whose thickness is $2(d + w_2(x_1,t))$ are written in the time domain as

$$\begin{aligned} &\frac{1}{\rho_f}\nabla P + \frac{D\boldsymbol{V}}{Dt} = 0, \\ &\frac{\partial}{\partial t}(\rho_f(d+w_2)) + \nabla\cdot(\rho_f(d+w_2)\boldsymbol{V}) = 0, \end{aligned} \tag{7}$$

where $\boldsymbol{V} = (V_1, V_2)$ and P are the velocity and pressure in the fluid, respectively, and D/Dt denotes the Lagrange derivative. For long wavelengths, the motion of the fluid is dominantly in the crack plane. In this study, following Chouet (1986), we thus assume that the fluid motion is one-dimensional in the crack plane and the fluid pressure is constant across the crack aperture. In addition, the advective terms are neglected under the assumption that these are small compared to the time derivatives of fluid pressure and velocities. Under these

assumptions, the governing equations for the fluid are written as

$$\begin{aligned}&\frac{1}{\rho_f}\frac{\partial P(x_1)}{\partial x_1}+\frac{\partial V_1(x_1)}{\partial t}=0,\\&\frac{1}{b}\frac{\partial P(x_1)}{\partial t}+\frac{\partial V_1(x_1)}{\partial x_1}+\frac{1}{d}\frac{\partial w_2(x_1)}{\partial t}=0,\end{aligned}\tag{8}$$

where b is the bulk modulus of the fluid. In the frequency domain, these equations become

$$\frac{\partial^2 P(x_1)}{\partial x_1^2}+\frac{\rho_f\omega^2}{b}P(x_1)+\frac{\rho_f\omega^2}{d}w_2(x_1)=0,\tag{9}$$

and the general solution of the equation is given by

$$P(x_1)=C_1e^{iA\omega x_1}+C_2e^{-iA\omega x_1}+\frac{i\omega}{2A}\frac{\rho_f}{d}\left\{e^{iA\omega x_1}\int_{-l}^{x_1}e^{-iA\omega\xi}\Delta w_2(\xi)d\xi-e^{-iA\omega x_1}\int_{-l}^{x_1}e^{iA\omega\xi}\Delta w_2(\xi)d\xi\right\},\tag{10}$$

where $A=\sqrt{\rho_f/b}=1/a$ is the slowness of the fluid, and C_1 and C_2 are the integral constants to be determined from the boundary conditions at the crack edges ($x_1=\pm l$).

Boundary conditions at the solid-fluid interfaces

The motions of the fluid inside the crack and the surrounding elastic solid as described above are coupled at the interfaces between the two regions. Such elastic coupling is represented by boundary conditions at the edges and surface of the crack.

The boundary condition at the crack edges, for the case where the crack is isolated and there is no external mass transfer, is the continuity of velocity of the elastic solid and that of the fluid. The condition is written as

$$V_1(x_1=\pm l)=i\omega w_1(x_1=\pm l),\tag{11}$$

and, by applying this boundary condition, we obtain the integral constants C_1, C_2 in Eq. (10) as

$$\begin{aligned}C_1=\frac{\rho_f\omega}{A}\frac{1}{e^{2iA\omega l}-e^{-2iA\omega l}}\Bigg[&e^{-iA\omega l}w_1(x_1=-l)-e^{iA\omega l}w_1(x_1=+l)\\&-\frac{1}{2d}\left\{e^{2iA\omega l}\int_{-l}^{+l}e^{-iA\omega\xi}\Delta w_2(\xi)d\xi+\int_{-l}^{+l}e^{iA\omega\xi}\Delta w_2(\xi)d\xi\right\}\Bigg],\\C_2=\frac{\rho_f\omega}{A}\frac{1}{e^{2iA\omega l}-e^{-2iA\omega l}}\Bigg[&e^{iA\omega l}w_1(x_1=-l)-e^{-iA\omega l}w_1(x_1=+l)\\&-\frac{1}{2d}\left\{\int_{-l}^{+l}e^{-iA\omega\xi}\Delta w_2(\xi)d\xi+e^{-2iA\omega l}\int_{-l}^{+l}e^{iA\omega\xi}\Delta w_2(\xi)d\xi\right\}\Bigg].\end{aligned}\tag{12}$$

The boundary conditions at the crack surface are the continuities of normal stress and normal displacement and the zero shear stress condition at the interface. Among these boundary conditions, those only on the normal and shear stresses need to be considered, since we are expressing motions of the elastic solid and the fluid using the crack surface displacement and thus the continuity of the normal displacement is automatically satisfied. Although these two boundary conditions are the general conditions for the interface between an elastic solid and an inviscid fluid, the conditions at the crack surface are further reduced to only the continuity of the normal stress on the crack surface when we consider a symmetric motion of the crack. This is because of the fact that symmetric motion of the crack surface yields $\tau_{12}=0$ on the crack plane ($x_2=0$), and due to the assumption of one-dimensional motion of the fluid, in case that the fluid is inviscid, $\tau_{12}=0$ on the crack surface ($x_2=\pm d$) is naturally satisfied.

Thus, we obtain following condition as the unique boundary condition at the crack surface.

$$\tau_{22}(x_1)=-P(x_1),\quad(|x_1|<l).\tag{13}$$

Here it should be noted that from Eqs. (5) and (10) the boundary condition Eq. (13) turns out to be a linear equation of the crack surface displacement $\Delta w_2(x_1)$.

3 NUMERICAL METHOD

As described in the previous section, the system of equations governing the motion of the fluid inside the crack and the surrounding elastic solid can be expressed by linear equations of the crack surface displacement, and thus the boundary condition at the crack surface is also represented by a linear function of the crack surface displacement. In the following, to determine the distribution of surface displacement which satisfies the boundary condition, we first rewrite the equations into a nondimensional form. We then expand the surface displacement using a set of continuous basis functions, and determine the weight of each basis function using the point collocation method so that the boundary conditions at the interfaces are satisfied.

3.1 Non-dimensionalization of the variables

In numerical computations, the equations and variables are expressed in dimensionless form through the following scaling

$$\begin{array}{lll} \text{Length} & : & r' = r \,/\, l \\ \text{Time} & : & t' = \beta t \,/\, l \end{array} \tag{14}$$

where the dimensionless variables are indicated by primes. Using the above scaling, other physical variables can also be recast in dimensionless form as

$$\begin{array}{lll} \text{Frequency} & : & \omega' = l\omega \,/\, \beta \\ \text{Displacement} & : & u' = \beta u \,/\, l^2 \\ \text{Stress} & : & \tau' = \beta\tau \,/\, (\mu l), \end{array} \tag{15}$$

and the equation for fluid pressure can be explicitly written as

$$\begin{aligned} P'(x',\omega') =& C_1 e^{im\omega' x'} + C_2 e^{-im\omega' x'} \\ &+ \frac{i\omega'}{2} mC \left\{ e^{im\omega' x'} \int_{-1}^{x'} e^{-im\omega'\xi'} \Delta w_2'(\xi') d\xi' - e^{-im\omega' x'} \int_{-1}^{x'} e^{im\omega'\xi'} \Delta w_2'(\xi') d\xi' \right\}, \\ C_1 =& i\omega' \frac{1}{m} \frac{\rho_f}{\rho} \frac{1}{e^{2im\omega'} - e^{-2im\omega'}} \left[e^{-im\omega'} \Delta w_1'(-1) - e^{im\omega'} \Delta w_1'(+1) \right. \\ &\left. - \frac{l}{2d} \left\{ e^{2im\omega'} \int_{-1}^{+1} e^{-im\omega'\xi'} \Delta w_2'(\xi') d\xi' + \int_{-1}^{+1} e^{im\omega'\xi'} \Delta w_2'(\xi') d\xi' \right\} \right] \\ C_2 =& i\omega' \frac{1}{m} \frac{\rho_f}{\rho} \frac{1}{e^{2im\omega'} - e^{-2im\omega'}} \left[e^{im\omega'} \Delta w_1'(-1) - e^{-im\omega'} \Delta w_1'(+1) \right. \\ &\left. - \frac{l}{2d} \left\{ \int_{-1}^{+1} e^{-im\omega'\xi'} \Delta w_2'(\xi') d\xi' + e^{-2im\omega'} \int_{-1}^{+1} e^{im\omega'\xi'} \Delta w_2'(\xi') d\xi' \right\} \right] \end{aligned} \tag{16}$$

where k and m are the ratios of wavenumbers defined by $k = k_\beta / k_\alpha$ and $m = k_a / k_\beta$ using the wave number of the acoustic wave in the fluid k_a. $C = b/\mu \cdot l/d$ in Eq. (16) is the crack stiffness (or the stiffness factor), first introduced by Aki et al. (1977) and which characterizes the response of a fluid-filled crack as extensively demonstrated by Chouet (1986, 1988).

3.2 Determination of the crack surface displacement

To determine the crack surface displacement which satisfies the boundary conditions, we first expand $\Delta w_2'(x_1')$ using the Chebyshev polynomial of the second kind U_i with a weight of $\sqrt{1 - x_1'^2}$, which is expressed as

$$\Delta w_2'(x_1') = \sqrt{1 - x_1'^2} \sum_{i=1}^{N_c} a_i U_{i-1}(x_1'), \qquad (|x_1'| \le 1), \tag{17}$$

where N_c is the number of polynomials considered and a_i is the coefficient of each polynomial. The use of the Chebyshev polynomial of the second kind has advantages both from the physical and mathematical point of views. Physically, the polynomial with the weight well describes the quasi-static behavior of crack deformation due to the internal pressure increase as demonstrated in Spence & Turcotte (1985). This is partly due to the mathematical property of the polynomial that the integral $\int_{-1}^{+1} \sqrt{1 - x^2} U_i(x)$ goes to 0 except for $i = 1$. Mathematically, the polynomial is nearly the same as the minimax polynomial.

After expanding the crack surface displacement using the polynomials, we then determine the coefficient of each polynomial a_i using the point collocation method (e.g., Banerjee & Butterfield, 1979) so that the boundary condition at the crack surface would be satisfied. In the present study, we use the same evenly-spaced collocation points for all polynomial degrees so that the coefficient of each polynomial can be determined by solving the following linear algebraic equation

$$e_i = \sum_{j=1}^{N_c} \Delta_{ij}\, a_j, \quad i = 1, \cdots, N_x \tag{18}$$

where N_x is the number of collocation points on the crack, e_i is the applied pressure at i-th collocation point ($x_1 = x_1^i$) and $\Delta_{ij} = \{\tau_{22}(x_1^i) + P(x_1^i)\}_j$ is the differential stress at $x_1 = x_1^i$ due to the crack surface displacement which is represented by the polynomial of degree j, respectively.

The important point to be noted is that since Eq. (18) is the general expression of the relation between the pressure (force) and the crack surface displacement, we can solve both free and forced oscillations of the fluid-filled crack using this equation. In the former case, the vector $\boldsymbol{e}$, which represents the applied force on the crack surface, is a null vector and we can obtain the complex eigen-frequencies and eigen-functions by solving the simultaneous equations. On the other hand, in the latter case, by putting an applied excitation pressure (force) to the vector $\boldsymbol{e}$ as a function of the location and frequency, we can solve the response of a fluid-filled crack. The use of Eq. (18) thus enables us to share the same computer code for both problems.

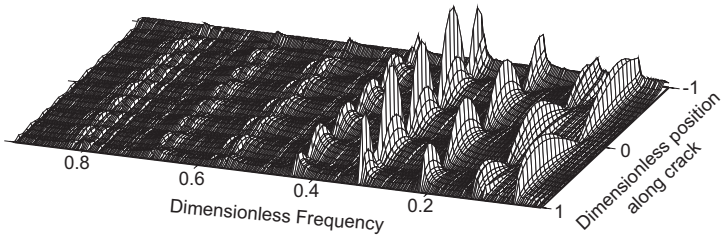

Figure 2. Spectral amplitude of the crack resonance. Spectral amplitude of the crack oscillation excited by a pressure change at $\frac{1}{4} = -1$ is shown as a function of the dimensionless frequency and position along the crack. Frequencies with high amplitude are the resonant frequency of the fluid-filled crack. Crack stiffness C is 50 and the material properties are $b/\mu = 0.5, \rho_f/\rho = 2/3, \lambda = \mu$.

3.3 Numerical evaluation of the integrals

The integrals in the system of equations for the elastic solid and the fluid are evaluated numerically. Since the Green's functions for the elastic solid have weak singularities as mentioned in the previous section, in order to achieve computational efficiency and avoid numerical instabilities caused by the cancellation of significant digits, we compute the integrands using the dynamic and static Green's functions (Eqs. (2) and (6)) depending on the value of $r^{'}$. In the present study, we use the dynamic Green's function for the range of $r^{'} > 10^{-4}$. For the range of $r^{'} \leq 10^{-4}$, we compute the integrands using both dynamic and static Green's functions in parallel, and once the result using the dynamic Green's functions agrees with that using the static ones, we stop computation of the dynamic ones. Afterward, the computation is carried out using only the static ones for smaller values of $r^{'}$.

4 NUMERICAL RESULTS

In this section, we present some typical examples using the above method. We focus here on the characteristics of the complex spectra of crack oscillations because the frequency and attenuation quality factor of the oscillation of a fluid-filled crack are key observational quantities to constrain the physical properties of the fluid inside the crack. In the following, since Eq. (18) is valid for both the excitation and the free oscillation problems, we consider the response of a fluid-filled crack from two different view points. First, we consider the response of a fluid-filled crack to an applied excitation, and investigate the frequency of the crack resonance: Second, we consider the free oscillation of a fluid-filled crack with no external applied force and investigate the attenuation of the crack resonance. In the previous studies using FDTD such as Chouet (1986), to avoid difficulties to satisfy the continuity of velocities between the elastic solid and the fluid at the crack edges, the fluid velocity is assumed to be zero at the edges. To keep consistency with these previous studies, in the following calculations, we enforce no-flow condition by putting $\Delta w_1'(x_1' = \pm 1) = 0$ in Eq. (16), although this condition is not necessarily required in the present method.

4.1 Resonance frequency

The oscillation of a fluid-filled crack caused by an applied excitation can be obtained by solving Eq. (18) by setting the appropriate excitation term $\boldsymbol{e}$ on the left-hand side of the equation. Figure 2 illustrates an example of the spectral characteristics of such a crack oscillation excited by a pressure change at one end of the crack ($x_1' = -1$). In the figure, the spectral amplitude is shown as a function of the dimensionless frequency and position along the crack. The frequencies with high spectral amplitudes represent the resonant frequencies of the crack oscillation and, in this example, the fundamental mode whose wavelength corresponds to the crack length ($\lambda' = 2$) and the first seven modes are clearly identified.

The frequencies of individual modes are easily measured from the spectral content of the forced oscillation as seen in Fig. 2. We can thus determine the dependency of resonance frequencies on the velocity and density of the fluid from successive computations with different fluid parameters. Figure 3 shows examples of dependency of resonant frequencies for two selected modes with wavelengths of $\lambda = 4l/3$ and $4l/5$. The range of the velocity ratio (α/a) and the density ratio (ρ/ρ_f) are chosen so that the properties of hydrothermal fluids and magmatic fluids are covered (e.g., Kumagai & Chouet, 2000). As shown in the figure, the resonance frequencies depend on both the velocity ratio and the density ratio, and the dependencies show different relations between modes. Such dependency of the resonant frequencies on the fluid properties was studied in detail by Kumagai & Chouet (2000) using FDTD, and our results are quite consistent with their results.

It is also possible to calculate the phase velocity of the crack wave propagating along the crack surface from the derived spectral amplitudes. That is, once the frequency and wavelength of the crack oscillation are obtained, we can calculate the phase velocity v_c of the crack wave using the formula $v_c/a = \beta/a \cdot \lambda' \cdot f'$. For instance, the dimensionless frequency and wavelength of the fundamental mode seen in Fig. 2 is $f' = 0.051$ and $\lambda' = 2$ respectively. Thus the phase velocity of the crack wave corresponding to the wavelength is obtained as $v_c = 0.117a$. This method to compute the phase velocity from the resonant modes was used to determine the dispersion relation of the crack wave by Chouet (1986) in his study using FDTD. In the next section, we will further discuss the determination of the dispersion relation of the crack wave by the present method.

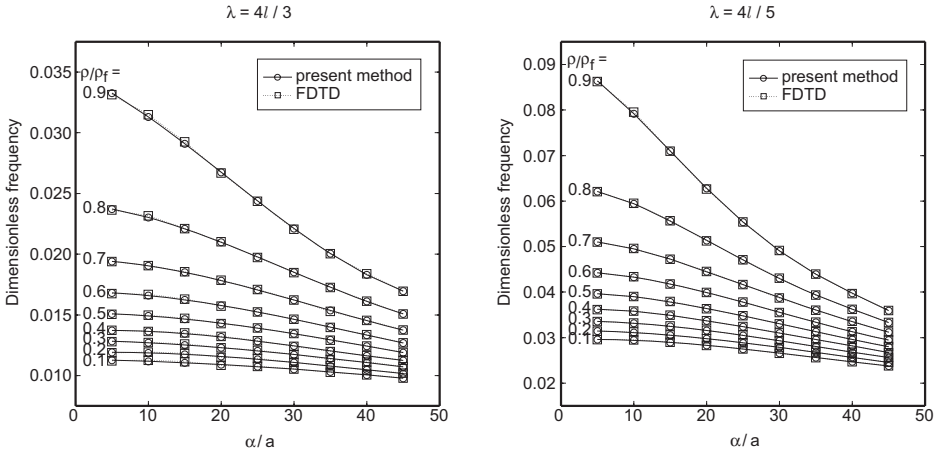

Figure 3. Dependency of the resonant frequencies on the fluid properties. The resonant frequencies of two modes ($\lambda = 4l/3, 4l/5$) are plotted as a function of the velocity ratio (α/a) and density ratio (ρ/ρ_f) by circles. Aspect ratio of the crack is fixed to $l/d = 10^4$. For comparison, those estimated from FDTD are also plotted by squares.

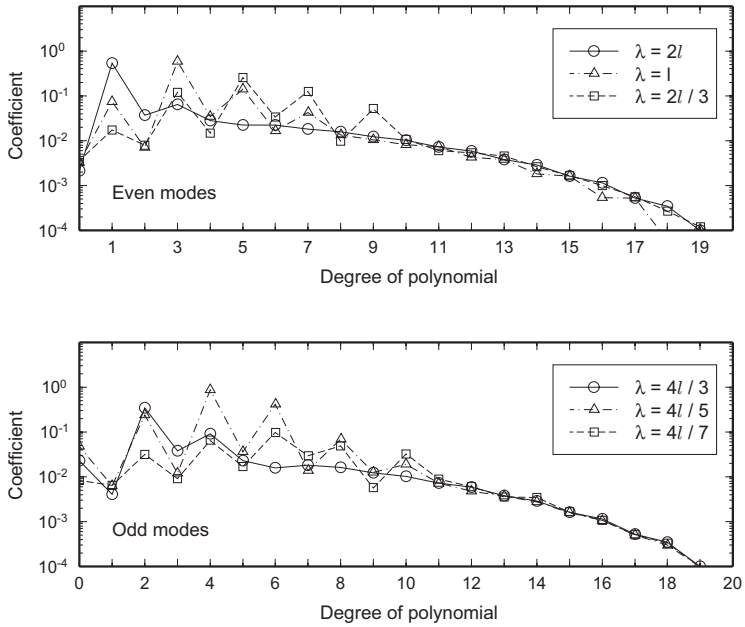

Figure 4. Coefficient of the polynomials used to expand each resonant mode. The crack parameters are same as those used in Fig. 2. Each coefficient is expressed in a unit of 10^2 (μ/l) $(\Delta w_2/\Delta P)$.

In the computation of this example, we use the Chebyshev polynomials of the degree up to 50 to expand the crack surface displacement. Figure 4 shows the coefficient a_i in Eq. (17) of the first twenty polynomials used to expand the lowest six resonant modes. As shown in the figure, odd-degree polynomials dominate in the even modes of crack oscillation whose wavelengths are $\lambda = 2l, l, 2l/3$, and even-degree polynomials dominate in the odd modes with wavelengths $\lambda = 4l/3, 4l/5, 4l/7$. This is because the Chebyshev polynomial of the second kind has an odd symmetry for odd degrees and an even symmetry for even degrees. Figure 4 also indicates that the higher-degree polynomials have smaller coefficients than lower-degree ones. Since the value of the polynomial of every degree falls within a range between -1 to 1 from its definition, the values of the coefficients directly reflect the contribution of each degree to form the modal shape. Based on these results, we conclude that it is sufficient to use only the lowest 30 polynomials in the simulations of the long-wavelength oscillations of a fluid-filled crack.

4.2 Resonance attenuation

The attenuation quality factor of crack resonance can be obtained from the complex eigen-frequencies of the free oscillations, which can be calculated by putting a null vector to the excitation term $\boldsymbol{e}$ in Eq. (18). Complex frequencies that yield $\det\Delta_{ij} = 0$ are the complex

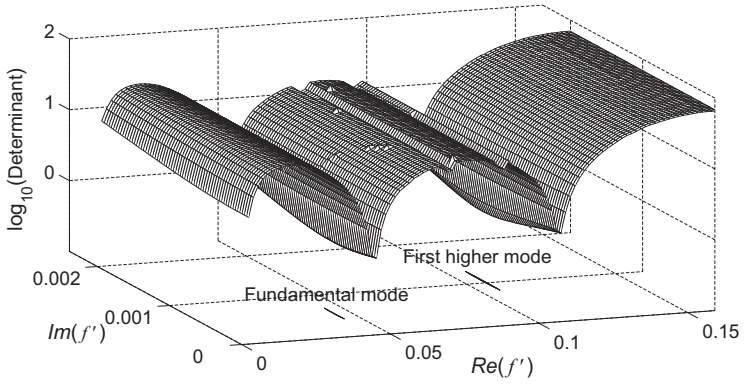

Figure 5. Determinant of the matrix Δ_{ij} as a function of the complex frequency: We use the grid search method to find the complex eigen-frequencies yielding $\det\Delta_{ij} = 0$. The complex eigen-frequencies are obtained by finding the minima of the determinant.

eigen-frequencies of the crack resonance. Each complex eigen-frequency $f + ig$ is related to the frequency f and the attenuation quality factor $Q(= f/2g)$ of resonant oscillation. Although, in general, the attenuation quality factor Q includes both the elastic radiation loss (Q_r) and intrinsic loss (Q_i) due to the viscous dissipation in the fluid, only Q_r appears in the present study because the fluid we are considering is purely inviscid.

Figure 5 shows an example of the determinant $\det\Delta_{ij}$ as a function of the complex frequency. The complex eigen-frequencies corresponding to the lowest two resonant modes are clearly seen in the figure. To find zeroes of the determinant of the matrix Δ_{ij}, we use the grid search method with fixed frequency steps in real and imaginary parts rather than relying on more sophisticated zero-finding algorithms. This is because the grid search method with fixed frequency steps allows for an efficient computation of the crack response for different material properties, as mentioned later. Therefore, the complex eigen-frequencies are obtained as frequencies yielding the minimum values of the determinant rather than exact zeroes (see Figure 5). In the present study, we use the frequency steps of 5×10^{-4} and 10^{-5} for the real and imaginary parts of the nondimensional complex frequency.

5 DISCUSSION

5.1 Efficiency of the method

In the present method, the response of the fluid-filled crack is calculated by determining the crack surface displacement so that the continuity of the normal stress in the elastic solid τ_{22} and the fluid pressure P is satisfied on the crack surface using the collocation method (see Eqs. (17) and (18)). Since the normal stress in the elastic solid and the fluid pressure can be computed separately using Eqs. (5) and (10), we can store and reuse these results as far as the material properties are kept unchanged. For example, when computing the response of a fluid-filled crack for different sets of fluid parameters with fixed parameters in the elastic solid, the normal stress τ_{22} on the crack surface due to the crack surface displacement represented by each degree of the polynomial can be used for all the computations with different fluid parameters; for each set of fluid parameters, we only need to evaluate the fluid pressure P on the crack surface using Eq. (10) and determine the crack surface displacement by solving the algebraic equation Eq. (18) whose size is just $N_x \times N_c$. In addition, the integration featured in the expression for the fluid pressure (Eq. (10)) has no singularity when the crack surface displacement is smooth, and thus the numerical evaluation of the integral can be carried out at very small computational cost. These features leads to an efficient and systematic computation of the dynamic response of a fluid-filled crack having various sets of fluid parameters with minimum computational cost as compared to domain-type methods like FDTD.

5.2 Comparison with FDTD

Resonance frequency and crack wave dispersion

A comparison of resonant frequencies of a fluid-filled crack computed by the present method and FDTD is shown in Fig. 3 for two resonant modes with wavelengths $\lambda = 4l/3$ and $4l/5$. The range of the velocity ratio and density ratio presented in this figure is selected so that most of the fluid properties that appear in volcanic environments including magmatic fluid and geothermal ones would be covered. As shown in the figure, the resonant frequencies obtained by the two different methods are consistent with each other over the parameter range of interest. Extensive tests with different crack parameters (not shown here) indicate that both methods give the same resonance frequencies and dispersion relations with little difference in the low frequency range.

Regarding to the dispersion relation of the crack wave, however, there is an additional advantage of the present method. In the previous

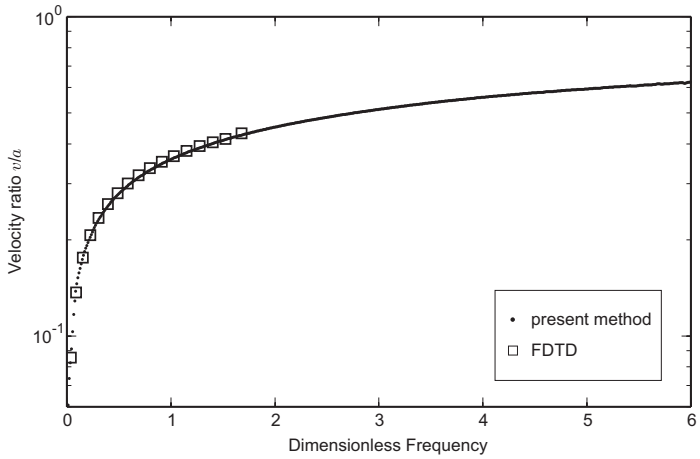

Figure 6. Dispersion relations obtained by the matrix pencil method (present method) and the direct measurement of the spectra (FDTD). Crack stiffness C is 100 and the properties of the materials are $b/\mu = 0.5, \rho_f/\rho = 2/3, \lambda = \mu$.

studies using FDTD, the dispersion relations are obtained from the frequencies and corresponding wavenumber, and these are directly measured from the spectra of the crack oscillation due to an applied excitation as described in the previous section. In this method, estimations of the phase velocity are restricted to the well-established resonant modes, and it is rather difficult to measure dispersion relations corresponding to the higher-degree modes due to their weak excitation. In the present method, however, since we can compute the phase of the propagating wave at arbitrary point on the crack surface once the displacement on the crack surface is determined, it is thus possible to calculate the phase velocity at any frequency of interest. This is done here by using the modified matrix pencil method (e.g., Hua & Sarkar, 1990). Figure 6 shows an example of the dispersion relation obtained by the present method and that obtained by the direct measurement of the spectra computed by FDTD. In contrast to the results from FDTD, the present method yields a continuous dispersion curve over a wide range of frequencies. Although only low-frequency modes have been considered in studies of volcanic signals so far, the computation of the dispersion relation over a wide frequency range may be useful in future applications such as the inversion of a crack excitation from observed seismograms in which the response over wide frequency range is required.

Resonance attenuation

In the previous studies (e.g., Kumagai & Chouet, 2000), the attenuation of crack oscillations was estimated by the Sompi method (e.g., Kumazawa et al., 1990) using various values of trial AR orders applied to the far-field waveform radiated from the fluid-filled crack. Results based on FDTD occasionally show a lot of scatter, which makes a precise determination of the attenuation properties of the crack resonance challenging. In the present method, the attenuation quality factor Q is directly calculated from the complex frequency of the eigen mode identified from the simultaneous equation (Eq. (18)). Such computations in the complex frequency domain enable us to compute a single estimate of the attenuation quality factor Q. Although this approach is more direct compared to FDTD, relatively broad minimum for the imaginary part of the complex frequency (see Fig. 5) suggests that this method yields the attenuation quality factors Q with limited precision as well. There is, however, a more significant limitation of FDTD in the estimation of the attenuation quality factor Q. To suppress numerical instabilities at short wavelengths caused by the discretization in the time and space, Chouet (1986) added an artificial dissipation term in the form of $c\nabla v$ to the equations of motion, where v is the velocity of either the elastic solid or the fluid. The factor c is a nondimensional dissipation coefficient, and Chouet (1986) assigned $c = 0.025$ in the elastic solid and $c = 0.075$ in the fluid as optimal values. Although this kind of dissipation term is commonly used in FDTD computations, the factor acts as a pseudo-viscosity that affects the estimation of attenuation properties of the crack oscillation.

In the 2-D problem, the effect of the dissipation term added to the equation for the fluid can be quantitatively evaluated as follows: Adding the term $c\nabla v$ to the nondimensional equation is equivalent to changing the equation of conservation of momentum as

$$\frac{1}{\rho_f}\frac{\partial P}{\partial x_1} + \frac{\partial V_1}{\partial t} - \left\{ c\left(\frac{a}{\alpha}\right)^2 \frac{2l\alpha}{N} \right\} \frac{\partial^2 V_1}{\partial x^2} = 0, \tag{19}$$

where N is a number of grid points used to discretize the crack length $2l$. Since the general solution of Eq. (19) can be also written as a linear function of the crack surface displacement just like the case of pure inviscid fluid, we can evaluate the effect of the artificial dissipation term by the same methodology as described in the previous section.

Figure 7(a) shows the effect of the artificial dissipation term on the attenuation quality factor Q of the crack resonance and its dependency on the value of the dissipation coefficient c. In the example, we use $\rho_f/\rho = 0.3$ and $\alpha/a = 10$ corresponding to the properties of a water-gas mixture. The figure clearly shows that the attenuation quality factor Q estimated from FDTD is affected by the value of c. Figure 7(b) illustrates the dependence of the attenuation quality factor Q on the value of c obtained by both FDTD and the present method using Eq. (19).

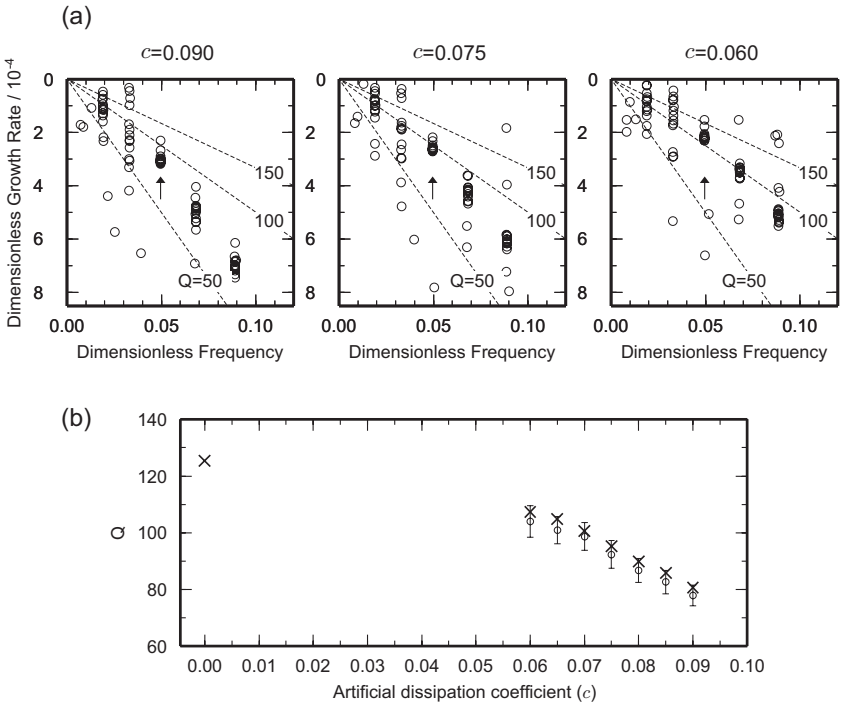

Figure 7. Effect of the artificial dissipation term. (a) Results of Sompi analyses of FDTD waveforms obtained with three different values of c. Circles represent the wave elements for all the trial AR orders between 8 and 20. Clusters of circles represent signals; for example, the cluster identified by the arrow represents the mode with $\lambda = 4l/5$. Dashed lines represent lines along which Q are constant. (b) Dependency of the attenuation quality factor Q on the artificial dissipation coefficient, c, for the mode with wavelength $\lambda = 4l/5$. Circles represent the values estimated by FDTD, and the crosses represent the values estimated by the present method. The value $c = 0$ represents the case where no artificial dissipation term is added to the governing equation. The value of c used in Chouet (1986) is 0.075, and the result of FDTD becomes unstable with the smaller value of c below 0.06.

There are small differences between the results obtained by the two methods, which may be partly due to the dissipation term added to the elastic solid equation. Nevertheless, the results of FDTD with small value of c approach the result derived from the present method without any artificial term ($c = 0$). Overall, our simulation of the effect of c using Eq. (19) adequately describes the behavior of FDTD results.

Our results suggest that the attenuation quality factor Q obtained by FDTD, which is used to estimate fluid properties in the previous studies, is underestimated due to the artificial term. The bias may become especially significant in the estimation of the attenuation quality factor Q for a crack containing bubbly water or water-bubble mixture. This is because its resonant frequency is not so sensitive to the mixing ratio of the bubbles, while the attenuation strongly depends on the composition of the fluid as demonstrated by Kumagai & Chouet (2000). This discrepancy may be also crucial in the discussion of the excitation efficiency of the resonance discussed in Fujita & Ida (2003), in which the attenuation characteristics of the resonance of spherical fluid inclusion and fluid-filled crack are compared based on the attenuation factor estimated by FDTD.

6 CONCLUSION

We proposed a simple and efficient method to simulate the dynamics of a fluid-filled crack embedded in a 2-D infinite elastic solid medium using the boundary integral method. The method is well-suited to the systematic investigation of the response of a crack over a wide range of medium parameters.

Our numerical tests demonstrate that the present method is capable of precisely computing both frequency and attenuation quality factor of the resonance of a fluid-filled crack. The resonant frequencies computed by the present method are consistent with those obtained by FDTD over the parameter range of interest. However, the two methods yield slightly different values of the attenuation quality factor of the resonant oscillation. It is revealed that the difference is mainly due to the artificial dissipation term used in FDTD, and the effect of the term is successfully estimated by the inclusion of an equivalent term in the present formulation. The results also demonstrate the flexibility of the present method in treating various situations other than that for a simple pure inviscid fluid case.

The advantages of the present method over FDTD can be summarized as follows: (1) The frequency domain computation enables us to evaluate a single estimate of the attenuation of the crack resonance directly from the complex eigen-frequency; (2) part of the computation results can be re-used because the motions of the elastic solid and fluid regions are separately computed as the functions of the crack surface displacement, and thus the systematic simulations of a fluid-filled crack with various fluid parameters can be performed at little additional

computational cost; (3) use of smooth continuous functions to represent the crack surface displacement avoids the numerical dispersion at short wavelengths inherent to FDTD; and (4) more realistic fluids with frequency-dependent properties can be easily implemented.

Although the model demonstrated in this paper is the simplest one, these advantages may enable us to incorporate various factors required for constructing realistic models of the volcanic seismic signals. The extensions of the method may include the inversion of the crack surface displacement from observed waveforms. So far, we have only undertaken forward modeling of the crack response. However, using the method described in this paper, we can determine the complex eigen-frequencies and eigen-functions of the crack resonance efficiently. It may thus be possible to invert the crack motion from the observed data. Such inversion may also give us information on the location and time history of the excitation forces, and enable us to infer more detailed image of the fluid dynamics beneath active volcanoes.

ACKNOWLEDGMENTS

We are grateful to Bernard Chouet and Simone Cesca for thorough reviews and constructive comments which help us significantly improve the manuscript. This work is partially supported by a grant from the Ministry of Education, Culture, Sports, Science, and Technology (MEXT) of Japan.

References

Aki, K. & Richards, P., 2002. *Quantitative Seismology, 2nd ed.*, University Science Books, Sausalito.

Aki, K., Fehler, M., & Das, S., 1977. Source mechanism of volcanic tremor: Fluid-driven crack models and their application to the 1963 Kilauea eruption, *J. Volcanol. Geotherm. Res.*, **2**, 259-287.

Banerjee, P. K. & Butterfield, R., 1979. *Developments in boundary element methods*, Elsevier Applied Science Publishers, London.

Benites, R., Aki, K., & Yomogida, K., 1992. Multiple scattering of sh waves in 2-D media with many cavities, *Pure Appl. Geophys.*, **138**, 353-390.

Biot, M. A., 1952. Propagation of elastic waves in a cylindrical bore containing a fluid, *J. Appl. Phys.*, **23**(9), 997–1005.

Carcione, J. M., Cavallini, F., Mainardi, F., & Hanyga, A., 2002. Time-domain modeling of constant-Q seismic waves using fractional derivatives, *Pure Appl. Geophys.*, **159**, 1719-1736.

Chouet, B., 1985. Excitation of a buried magmatic pipe: a seismic source model for volcanic tremor, *J. Geophys. Res.*, **90**, 1881-1893.

Chouet, B., 1986. Dynamics of a fluid-driven crack in three dimensions by the finite difference method, *J. Geophys. Res.*, **91**, 13967-13992.

Chouet, B., 1988. Resonance of a fluid-driven crack: Radiation properties and implications for the source of long-period events and harmonic tremor, *J. Geophys. Res.*, **93**, 4375-4400.

Chouet, B., 2003. Volcano seismology, *Pure Appl. Geophys.*, **160**, 739-788.

De Angelis, S. & McNutt, S. R., 2005. Degassing and hydrothermal activity at Mt. Spurr, Alaska during the summer of 2004 inferred from the complex frequencies of long-period events, *Geophys. Res. Lett.*, **32**, L12312.

Ferrazzini, V. & Aki, K., 1987. Slow waves trapped in a fluid-filled infinite crack: Implication for volcanic tremor, *J. Geophys. Res.*, **92**, 9215-9223.

Ferrick, M., Qamar, A., & Lawrence, W. F. S., 1982. Source mechanism of volcanic tremor, *J. Geophys. Res.*, **87**, 8675-8683.

Fujita, E. & Ida, Y., 2003. Geometrical effects and low-attenuation resonance of volcanic fluid inclusions for the source mechanism of long-period earthquakes, *J. Geophys. Res.*, **108**, 2118.

Fujita, E., Ida, Y., & Oikawa, J., 1995. Eigen oscillation of a fluid sphere and source mechanism of harmonic volcanic tremor, *J. Volcanol. Geotherm. Res.*, **69**, 365-378.

Hua, Y. & Sarkar, T. K., 1990. Matrix pencil method for estimating parameters of exponentially damped/undamped sinusoids in noise, *IEEE Trans. Acoust., Speech, Signal Processing*, **38**, 814-824.

Kawakatsu, H. & Yamamoto, M., 2007. *Volcano Seismology* in *Treatise on Geophysics*, vol. 4, edited by H. Kanamori, Elsevier.

Kawakatsu, H., Kaneshima, S., Matsubayashi, H., Ohminato, T., Sudo, Y., Tsutsui, T., Uhira, K., Yamasato, H., Ito, H., & Legrand, D., 2000. Aso94: Aso seismic observation with broadband instruments, *J. Volcanol. Geotherm. Res.*, **101**, 129-154.

Krauklis, P. V., 1962. On low-frequency oscillations of a liquid layer in an elastic medium, *Prikladnaya Matematika i Mekhanika (J. Appl. Math. Mech.)*, **26**, 1111–1115.

Kumagai, H. & Chouet, B. A., 2000. Acoustic properties of a crack containing magmatic or hydrothermal fluids, *J. Geophys. Res.*, **105**, 25493-25512.

Kumagai, H., Chouet, B. A., & Nakano, M., 2002. Temporal evolution of a hydrothermal system in Kusatsu-shirane volcano, Japan, inferred from the complex frequencies of long-period events, *J. Geophys. Res.*, **107**, ESE 9-1.

Kumagai, H., Miyakawa, K., Negishi, H., Inoue, H., Obara, K., & Suetsugu, D., 2003. Magmatic dike resonances inferred from very-long-period seismic signals, *Science*, **299**, 2058-2061.

Kumazawa, M., Imanishi, Y., Fukao, Y., Furumoto, M., & Yamamoto, A., 1990. A theory of spectral analysis based on the characteristic property of a linear dynamic system, *Geophys. J. Int.*, **101**, 613-630.

Molina, I., Kumagai, H., & Yepes, H., 2004. Resonances of a volcanic conduit triggered by repetitive injections of an ash-laden gas, *Geophys. Res. Lett.*, **31**, L03603.

Randall, C. J., 1991. Modes of noncircular fluid-filled boreholes in elastic formations, *J. Acoust. Soc. Am.*, **89**, 1002-1016.

Sakuraba, A., Oikawa, J., & Imanishi, Y., 2002. Free oscillations of a fluid sphere in an infinite elastic medium and long-period volcanic earthquakes, *Earth Planets Space*, **54**, 91-106.

Schoenberg, M. & Sen, P. N., 1983. Properties of a periodically stratified acoustic half-space and its relation to a biot fluid, *J. Acoust. Soc. Am.*, **73**, 61–67.

Spence, D. & Turcotte, D. L., 1985. Magma-driven propagation crack, *J. Geophys. Res.*, **90**, 575-580.

Yamamoto, M., Kawakatsu, H., Kaneshima, S., Mori, T., Tsutsui, T., Sudo, Y., & Morita, Y., 1999. Detection of a crack-like conduit beneath the active crater at Aso volcano, Japan, *Geophys. Res. Lett.*, **26**, 3677-3680.